The role of the austenite grain size in the martensitic transformation in low carbon steels

Alonso de Celada Casero, Carola; Sietsma, Jilt; Santofimia Navarro, Maria

DOI
10.1016/j.matdes.2019.107625

Publication date
2019

Document Version
Final published version

Published in
Materials and Design

Materials and Design 167 (2019) 107625

Contents lists available at ScienceDirect

Materials and Design

journal homepage: www.elsevier.com/locate/matdes

The role of the austenite grain size in the martensitic transformation in low carbon steels

Carola Celada-Casero *, Jilt Sietsma, Maria Jesus Santofimia

Department of Materials Science and Engineering, Delft University of Technology, Mekelweg 2, 2628CD Delft, the Netherlands

HIGHLIGHTS

- The nuclei density and the thermodynamic balance between chemical driving force and austenite strength determine the martensite transformation rate
- Grain refinement increases the austenite resistance against the austenite/martensite interface motion and suppresses strain relaxation mechanisms
- Austenite grain refinement lowers the MS and increases the initial transformation rate through the repeated nucleation of parallel martensite laths
- After approximately a 30% of martensite has formed, the transformation rate decreases rapidly for small prior austenite grain sizes

GRAPHICAL ABSTRACT

The austenite grain size influences the martensitic transformation through the nuclei density provided by the grain boundary area and through the strengthening of the austenite phase as the transformation progresses.

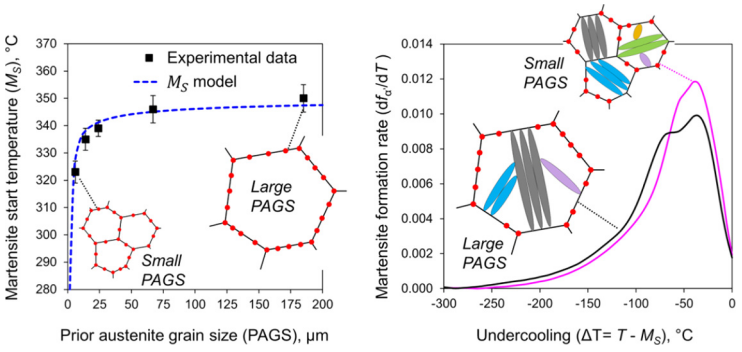

ARTICLE INFO

Article history:
Received 26 November 2018
Received in revised form 24 January 2019
Accepted 26 January 2019
Available online 29 January 2019

Keywords:
Prior austenite grain size
Martensite
Austenite
Lath aspect ratio
Transformation kinetics
Steels

ABSTRACT

There is sufficient experimental evidence to propose that the formation kinetics of athermal martensite directly depends on the austenite grain structure from which the martensite forms. Yet, this dependence is frequently ignored. The present study investigates the role of the prior austenite grain size (PAGS) in the martensitic transformation in low-carbon steels. The transformation kinetics was experimentally studied for PAGS in the range from 6 to 185 μm and theoretically analysed based on the nucleation rate and the thermodynamic balance between the chemical driving force and the resistance exerted by the austenite against the progress of the transformation. It is observed that grain refinement shifts the martensite start temperature (M_S) to lower values and accelerates the transformation rate at initial stages. At a later stage, when approximately 30% martensite has formed, the transformation rate decreases rapidly for small PAGS, whereas higher rates are maintained in coarse-grained microstructures. The change in martensite formation rate with the grain size depends on the nuclei density and on the austenite strength. This research enables an optimised selection of processing parameters for the design of ultra-high strength steels that require the formation of a controlled fraction of martensite.

1. Introduction

The formation of martensite is exploited in a number of advanced high-strength steels (AHSSs) in which martensite is used as main strengthening constituent in combination with a ductile phase, like

* Corresponding author.
E-mail addresses: C.CeladaCasero@tudelft.nl (C. Celada-Casero), J.Sietsma@tudelft.nl (J. Sietsma), M.J.SantofimiaNavarro@tudelft.nl (M.J. Santofimia).

https://doi.org/10.1016/j.matdes.2019.107625

ferrite or austenite [1], and to improve performance properties as formability and fracture toughness [2]. Examples are dual-phase (DP), complex-phase (CP), transformation-induced plasticity (TRIP) and Quenching and Partitioning (Q&P) steels. Understanding the influence of the steel processing parameters on the martensite start temperature (M_S) and martensite formation kinetics is crucial either to avoid the formation of martensite during thermal or thermo-mechanical treatments, like during the isothermal formation of bainite in carbide-free bainitic steels [3], or to exert control of the volume fraction of martensite to be formed, like in Q&P processing routes [4] and other strategies for the creation of AHSSs [5].

Martensite has been extensively studied in steels [6–19]. Yet, our knowledge about the exact mechanisms by which martensite nucleates and grows is very limited. Christian and Entwisle [8,15] described the formation kinetics of athermal martensite as mainly dependent on the nucleation stage as the growth of the plates is extremely fast and therefore seems to be independent of time. The formation of athermal martensite can only occur at a certain degree of undercooling below the temperature at which the Gibbs free energy of martensite and austenite is the same for a given composition (T_0). The degree of undercooling depends on the balance between the negative contribution to the free energy change due to the transformation and the positive contribution due to processes opposing the transformation, like transformation strain. Once the favourable energy balance is reached at the M_S temperature, the martensite plates grow following a diffusionless mechanism where the fraction of formed martensite depends on the undercooling below M_S [20]. In addition to these thermodynamic considerations, kinetically the activation energy for nucleation plays a role. The most well-known and accepted mechanism for the heterogeneous nucleation of bcc-martensite in fcc-austenite was proposed by Olson and Cohen [9,10]. They suggested a barrier-less nucleation process on pre-existing defects by dissociation of groups of dislocations provided the driving force is sufficient. However, the exact mechanism by which this occurs is not clear yet. The exact atomic displacements that lead to the fcc-to-bcc crystal structure change in pure iron have recently been investigated by molecular dynamics simulations, concluding that several types of martensitic transformation mechanism can occur, depending on the type of defects present in the parent austenite [21]. The growth rate of each plate is then controlled by the mobility of the semi-coherent interface that exists between the nucleus and the austenite. Based on Olson and Cohen's theory, Ghosh and Olson [13,14] developed their model to calculate the critical driving force for an fcc-to-bcc transformation.

Among all processing parameters that might influence the athermal martensitic transformation, it is of great importance to understand the effect of the austenitisation conditions as they lead to the prior austenite grain structure (including the prior austenite grain size, PAGS) from which the martensite will form. Morphological and kinetic aspects of the martensite formation depend directly on the PAGS. It is frequently observed experimentally that austenite grain refinement leads to a decrease in the M_S temperature. Variations of about 40 °C have been reported for austenite grain size reductions from about 100 μm to a few micrometres in low carbon steels [22,23]. The effect was identified by Ansell and co-workers [24,25] to originate from the grain-size dependence of the resistance of the austenite against plastic deformation. Since then, several empirical equations have been proposed in the literature in order to predict the influence of the prior austenite grain size on the M_S temperature [20,22,26,27]. However, all these equations involve fitting parameters with no clear physical meaning. Although the martensite transformation kinetics is very frequently considered to be only composition dependent, there is sufficient experimental evidence [22–28] to suggest that it actually depends on the nucleation rate and the energy balance between the chemical driving force and the resistance exerted by the austenite against the transformation. These factors do not only depend on the composition, but are directly influenced by the PAGS.

In this study, the influence of the prior austenite grain size (PAGS) on the formation process of athermal martensite is investigated in a low-carbon steel. The transformation kinetics is experimentally studied by dilatometry, and theoretically analysed applying the Koistinen-Marburger kinetic equation and a thermodynamics based model that considers the effect of the PAGS on the martensite start temperature (M_S). Variations in the martensite start temperature and the transformation kinetics with the PAGS are explained based on the austenite strength and the work exerted by the austenite against the martensite/austenite interface motion.

2. Material and experimental procedure

A 0.2C-3.5Mn-1.5Si-0.5Mo (wt. %) steel is investigated. The steel was supplied in the form of 4 mm thick hot-rolled strips. Cylindrical samples of 10 mm in length and 3.5 mm in diameter were machined parallel to the rolling direction (RD) and heat-treated in a Bähr DIL 805A/D dilatometer under vacuum. Dilatometry showed starting resp. finishing austenitisation temperatures (A_{C1} resp. A_{C3}) of 720 resp. 880 °C at a heating rate of 5 °C/s. Microstructures with varying PAGS were created by applying two different annealing strategies (Fig. 1). In the first set of heat treatments (Fig. 1a), the material was heated above the A_{C3} temperature and held for 240 s. The PAGS was varied by selecting the austenitisation temperature (T_γ) in the range 900 to 1200 °C in intervals of 100 °C. In the second set of heat treatments (Fig. 1b), the PAGS was refined through thermal cycling [29], which includes a set of three thermal cycles after austenitisation at 900 °C for 240 s. In each cycle, the microstructure is rapidly heated to 900 °C, held for 3 s and transformed back into martensite by cooling to room temperature at 50 °C/s. This increases the density of austenite nucleation sites for the next cycle and results in a refinement of the grains size. In total, five different PAGS were produced. The effect of the PAGS on the martensitic transformation was investigated based on the dilatometry curves obtained during cooling to room temperature at 50 °C/s. For statistical purposes, per PAGS condition a mean dilatometry curve was considered by averaging at least three dilatometry experiments. The uncertainty was calculated based on the standard deviation among curves at each temperature.

Magnetisation saturation measurements using a LakeShore 7307 VSM magnetometer were carried out at room temperature in discs of 2 mm in thickness cut out from the centre of the dilatometry specimens. The magnetisation saturation value (${M_{sat}}^{PAGS}$) of the specimen allows to determine the volume fraction of martensite present in the microstructure after quench as $f_{\alpha'} = {M_{sat}}^{PAGS}/{M_{sat}}^{\alpha'}$, where ${M_{sat}}^{\alpha'}$ corresponds to the magnetisation saturation of martensite. This value can be theoretically calculated as ${M_{sat}}^{\alpha'} = x_{Fe}{M_{sat}}^{\alpha-Fe}$, where x_{Fe} is the iron content of the steel in wt. % and ${M_{sat}}^{\alpha-Fe}$ is the magnetisation saturation of pure bcc-Fe, which yields 215 Am^2/kg at room temperature [30].

The PAGS was revealed by the thermal etching method [31]. Flat specimens, 10 mm long, 5 mm wide and 2 mm thick, were prepared with one of the faces carefully polished down to 1 μm and were heat treated in the furnace of the Bähr DIL 805A/D dilatometer as represented in Fig. 1. Due to thermal etching, grooves of approximately 1–2 μm in width form during austenitisation at the intersection of the austenite grain boundaries (PAGB) and the free polished surface due to preferential transfer of matter away from the grain boundary [31]. Groove formation creates a good contrast between the boundary and the inner part of the grain. Therefore, chemical etching is not needed. The grain size was determined by manually tracing the grain boundaries on different micrographs using image-editing software (Photoshop) to create a skeleton outline. Between 300 and 600 prior austenite grains were analysed for each condition using the ImageJ software to determine grain areas and size distributions. Nomarski differential interference microscopy [31] under bright field illumination in an Olympus BX670M light optical microscope (LOM) gives good contrast in those conditions with large to intermediate PAGSs. Thermal etching did not

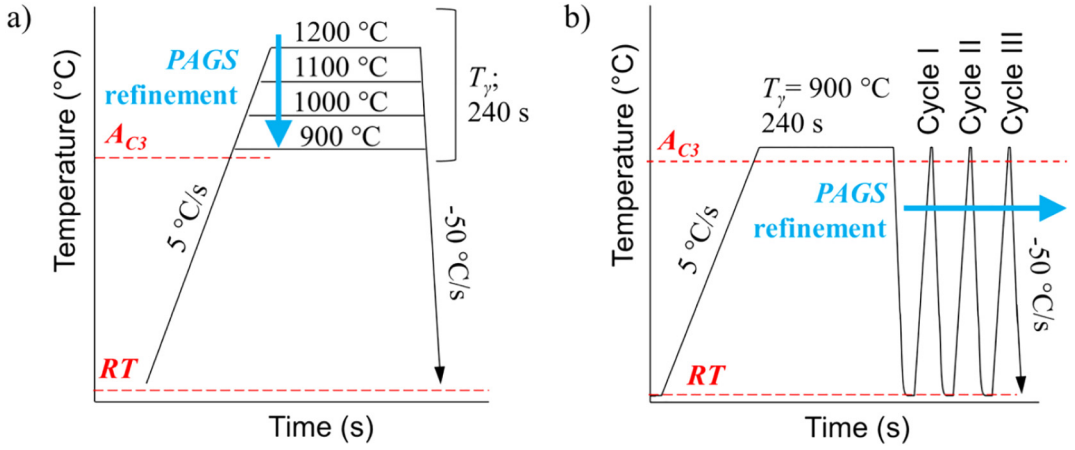

Fig. 1. Annealing schedules for the design of microstructures with different PAGS: (a) the austenitisation temperature (T_γ) is varied; (b) thermal cycling is included after austenitisation.

clearly reveal the PAGBs of the smallest grain size condition; band-contrast electron backscattered diffraction (EBSD) maps were used instead. EBSD analysis was also use to characterise morphological changes in the martensite substructure depending on the PAGS. Data acquisition was performed using a JEOL JSM-6500F scanning electron microscope operating at 20 kV, working distance of 25 mm and step size of 50 nm. Sample preparation included grinding, polishing down to 1 μm and a final polishing step with 0.05 μm OPS suspension for 15 min. The post-processing was done using Channel 5 software (Oxford Instruments).

3. Results

3.1. Microstructural characterisation

Fig. 2 shows a band-contrast EBSD map and optical micrographs after thermal etching and the corresponding grain size distributions. Average PAGS values of 6 ± 1 μm, 14 ± 1 μm, 25 ± 1 μm, 67 ± 1 μm and 185 ± 1 μm were obtained for the specimens subjected to thermal cycling and austenitisation at T_γ = 900 °C, 1000 °C, 1100 °C and 1200 °C, respectively. Normal grain size distributions are found for the conditions with the smaller grain sizes, whereas the distributions for intermediate and large sizes are asymmetric. In some micrographs (Fig. 2d–e) the martensite packets and blocks are made evident due to surface relief on the polished surface promoted by the martensitic transformation. This surface relief may mask the visualization of PAGBs when the grain size is small.

In order to get insight into morphological changes in the martensite substructure with grain size, the microstructures were analysed using EBSD. Martensite blocks were defined as bcc grains outlined by high angle grain boundaries (HAGBs), having a misorientation larger than 15°. The lath morphology was studied based on the blocks length and lath width, assuming the lath length equal to the block length. The

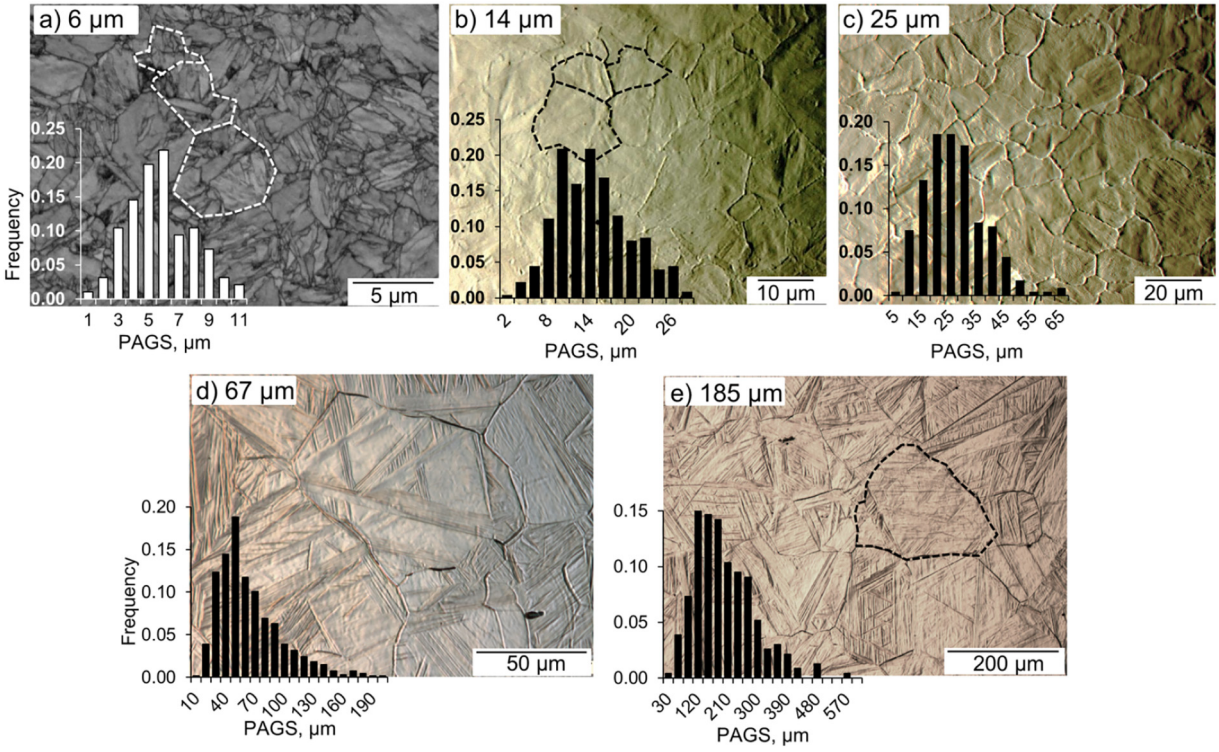

Fig. 2. (a) Band-contrast EBSD map and (b-e) LOM micrographs after thermal etching of the five different prior austenite grain sizes (PAGSs). The grain size distribution is shown in each case. The PAGS is expressed as the mean equivalent diameter and the standard deviation of the mean value, which is ±1 μm in all cases.

lath width was measured using misorientation profile lines drawn perpendicular to the expected lath habit plane in multiple martensite blocks and considering misorientations higher than 3° [32]. Average values between 0.20 and 0.24 μm (±0.02 μm) were found for all PAGS values, which is in good agreement with previous characterisation by transmission electron microscopy in low carbon steels [33]. Fig. 3 shows the distributions of c/a, the lath aspect ratio, for different PAGSs. The distribution peak is located at c/a values of 0.1 or lower for PAGS between 14 and 67 μm. The martensite structure resulting from a PAGS of 6 μm exhibits a much broader distribution and a peak at a higher c/a value. This indicates that austenite microstructures with PAGS below 14 μm give rise to more equiaxed martensite laths or, in other words, to higher c/a lath aspect ratios.

3.2. Dilatometry

Fig. 4a displays the average dilatometry response obtained during cooling for the different PAGSs. The expansion associated with the martensitic transformation shifts to lower temperatures as the PAGS decreases. Magnetisation saturation values of about 200 Am^2/kg were obtained at room temperature for all cases, which corresponds to a volume fraction of martensite of 0.99 ± 0.01. Fig. 4b shows that during thermal cycling the most pronounced decrease in M_S temperature occurs in the first cycle (Cycle I), as also observed by other authors [34]. The volume fraction of martensite phase was obtained by applying the lever rule to the average dilatometry curves, accounting for the expansion behaviour of the fcc and bcc lattices [35], and the experimental M_S is defined as the temperature at which a martensite volume fraction of 0.01 is formed. Fig. 4c depicts the evolution of the martensite volume fraction with temperature for the different PAGSs. A total decrease in the experimental M_S of 32 ± 5 °C is registered for a grain refinement from 185 to 6 μm. This magnitude is in good agreement with variations reported in the literature due to grain size reduction [22].

4. Discussion

4.1. Influence of austenite grain size on the martensite formation kinetics

The Koistinen-Marburger (KM) model [7] is usually employed to quantitatively describe the progress of the martensite volume fraction ($f_{\alpha'}$) with temperature during cooling. Here, it is used to study the effect of the PAGS on the kinetics of martensite formation:

$$f_{\alpha'} = 1 - exp[-\alpha_m(T_{KM} - T)] \quad (1)$$

where T_{KM} is the Koistinen-Marburger martensite start temperature and α_m is the overall rate parameter. Eq. (1) was fitted to the experimental curves. As the KM model does not adequately predict the early stages of the transformation, data below a martensite fraction of 0.15 were excluded from the fitting [18]. The obtained best fit parameters are shown in Table 1 along with the M_S values, for comparison. The extrapolated T_{KM} temperature is lower than the experimental M_S [17] and corresponds to the formation of a volume fraction of martensite of approximately 0.07 for each PAGS according to the dilatometry data. The rate parameter values are very close to the value calculated using the composition-dependent empirical equation proposed in [17], which is $\alpha_m = 0.0205\ K^{-1}$. Nevertheless, there is a clear increase of α_m with grain refinement down to 14 μm. This indicates that the overall rate parameter, which represents intermediate and final stages of the transformation, is affected by the PAGS. At PAGS lower than 14 μm a decreasing trend in α_m appears to occur.

Fig. 5a shows the comparison between the experimental kinetics and the KM fit for the smallest (6 μm), the largest (185 μm) and an intermediate PAGS (25 μm). The difference between M_S and the T_{KM} temperatures is plotted as a function of the PAGS in Fig. 5b. A maximum deviation of 20 °C is registered, which becomes smaller as the PAGS is reduced. This reveals that the formation of the martensite fraction corresponding to the T_{KM} temperature (0.07 in all cases) takes longer times in microstructures with PAGSs of 25 μm or above than in those with smaller PAGSs. This effect is known as "slow-start" phenomenon and was previously noted for high-carbon [18,36] and low-carbon [23] steels. The effect was recently attributed to the dispersion of M_S temperatures arising from local chemical inhomogeneities in a stainless steel [37]. However, why the slow-start magnitude decreases with the decrease of austenite grain size is not clear yet.

To understand the origin of the "slow-start" phenomenon the martensite transformation rate ($df_{\alpha'}/dT$) was calculated using the experimental kinetic curves. The M_S temperature is selected as onset temperature in order to suppress the effect of the PAGS on the undercooling required to initiate the transformation for each grain size. In this way, the kinetics can be directly compared. Fig. 6a shows the transformation rate as a function of the undercooling, $\Delta T = T - M_S$. Microstructures with small grain sizes reach the peak in transformation rate at lower undercooling values than microstructures with large grain sizes. It is worth mentioning that actually a double rate peak is observed for most of the curves, but it is especially pronounced for the PAGS of 185 μm. This effect is attributed to the released latent heat due to the exothermic martensitic transformation. As pointed out by Krisement et al. [38], the martensite formation rate is too high at the peak for the released latent heat to propagate through the material and thus it is locally dissipated. Then, the local temperature increases and slows down the transformation rate. This local temperature increase cannot be compensated by the temperature control of the dilatometer.

The general observed tendency in Fig. 6 is that the overall transformation rate increases with the decrease of PAGS. However, the highest transformation rate is observed for the PAGS of 14 μm and it decreases with further decreasing grain size. The reversion in the trend observed for the grain sizes of 6 μm and 14 μm results from the deviating trend among dilatometry experiments. This observation agrees well with the trend of the α_m parameter and, thus, it can be concluded that the overall transformation rate increases as the PAGS decreases, until a PAGS of 14 μm. After the peak, *i.e.* at larger undercooling, microstructures with large PAGSs sustain higher transformation rates than those with small PAGSs during a larger extent of undercooling. This can also be observed in Fig. 6b, where the martensite transformation rate is

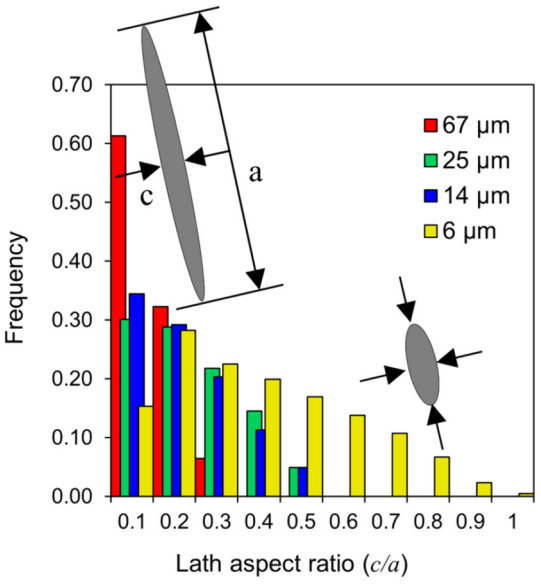

Fig. 3. Lath aspect ratio (c/a) distributions for different PAGSs. The ellipses represent martensite laths with a low and high aspect ratio.

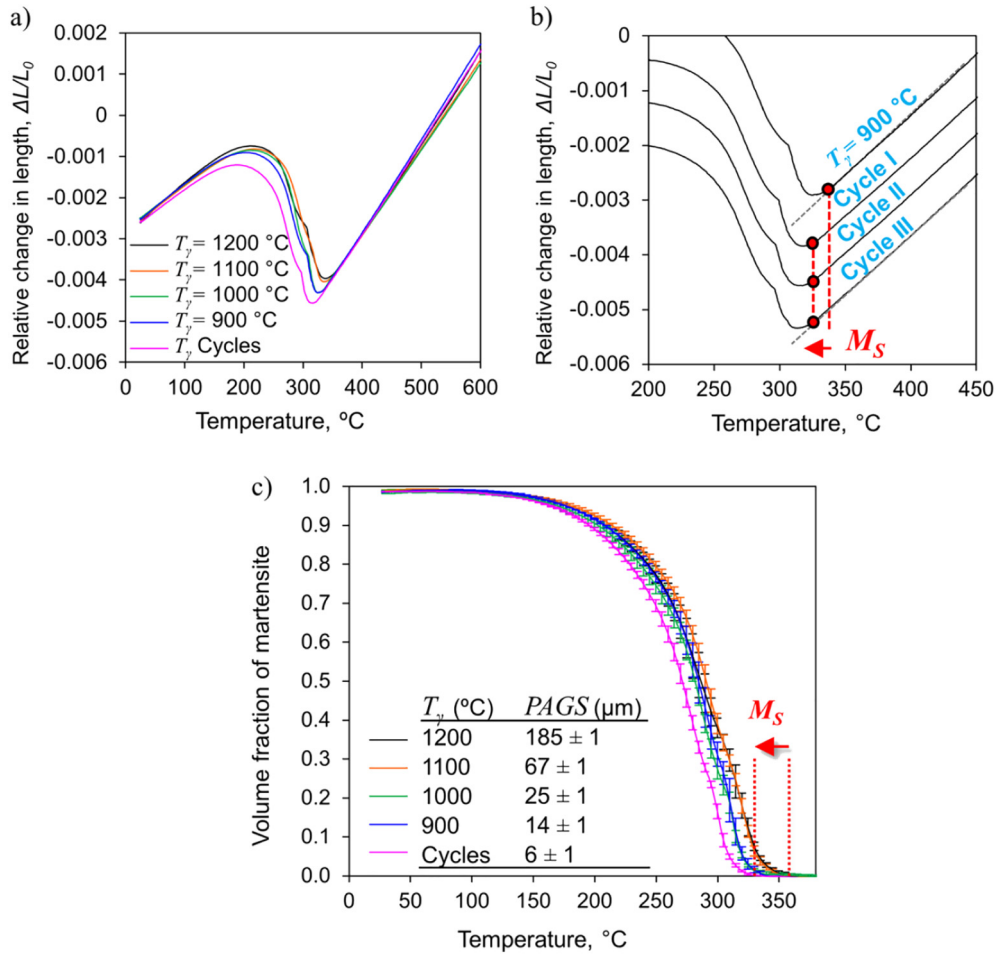

Fig. 4. (a) Dilatometry curves during cooling for the different PAGSs; (b) dilatometry curves during cooling steps of thermal cycling; (c) martensite volume fraction *vs.* temperature. Cycles stands for the specimen subjected to thermal cycling and T_γ for austenitisation temperature.

plotted against the volume fraction of martensite on a logarithmic scale in order to magnify the initial stages (small undercooling). From the M_S temperature, the transformation rate of microstructures with PAGSs above 25 μm is lower than that of microstructures with smaller PAGSs during the initial stages of the transformation. This means that the formation of the first martensite fraction takes longer times in microstructures with large PAGSs than in those with small PAGSs. Small PAGSs sustain higher transformation rates until a martensite fraction of around 0.60 has formed. The peak rate is achieved for a martensite fraction of around 0.30, irrespective of the PAGS. Fig. 6c shows the volume fraction of martensite against both undercooling and time once the transformation is initiated. Larger fractions of martensite are formed at fixed cooling times with decreasing the PAGS, which indicates a faster transformation kinetics. The influence of the transformation rate on the martensite fraction is more evident at intermediate-final stages of the transformation. However, it originates at the very initial stages of the transformation, when the austenite grain size due to differences of grain boundary area plays a role in the martensite nuclei density and hence in the transformation rate. This is the origin of the slow-start phenomenon with the increase of the PAGS.

The kinetics of the martensite formation is generally described considering the martensite nucleation rate and the volume of the martensite unit [22,28,39]. As revisited by Cohen in [12], the initiation of the transformation is controlled by pre-existing nucleation sites like grain boundaries; whereas the progress of the transformation depends on the interplay between pre-existing and autocatalytically generated defects. The analysis presented in Fig. 6 reveals two important effects of the PAGS on the martensite transformation kinetics, which are discussed hereafter and sketched in Fig. 7 for both cases a small and a large PAGS.

1. Grain refinement increases the *density of grain boundary nuclei*. Small-grained microstructures have a larger grain boundary area per unit of volume than coarse-grained microstructures and thus provide a higher density of pre-existing nucleation sites for the martensite. The first nucleation event increases the interfacial and elastic strain energy in the system due to the creation of an α′/γ interface and the volume misfit between martensite and austenite, respectively. In order to reduce the energy, the repeated nucleation of martensite laths at the α′/γ front is activated, which is known as autocatalytic effect [39]. In this study, the M_S temperature does not correspond to the first nucleation event, but to the smallest dilatometry-detectable fraction of martensite (0.01). Therefore, the progress of the transformation beyond a martensite fraction of 0.01 is controlled by the interaction between both pre-existing and

Table 1
Experimental details and results for different austenitisation treatments.

PAGS (μm)	M_S (°C)	T_{KM} (°C)	α_m (K^{-1})
6 ± 1	323 ± 4	308	0.0215 ± 0.0002
14 ± 1	335 ± 4	318	0.0219 ± 0.0004
25 ± 1	341 ± 3	318	0.0205 ± 0.0003
67 ± 1	349 ± 5	328	0.0207 ± 0.0002
185 ± 1	355 ± 5	330	0.0198 ± 0.0004

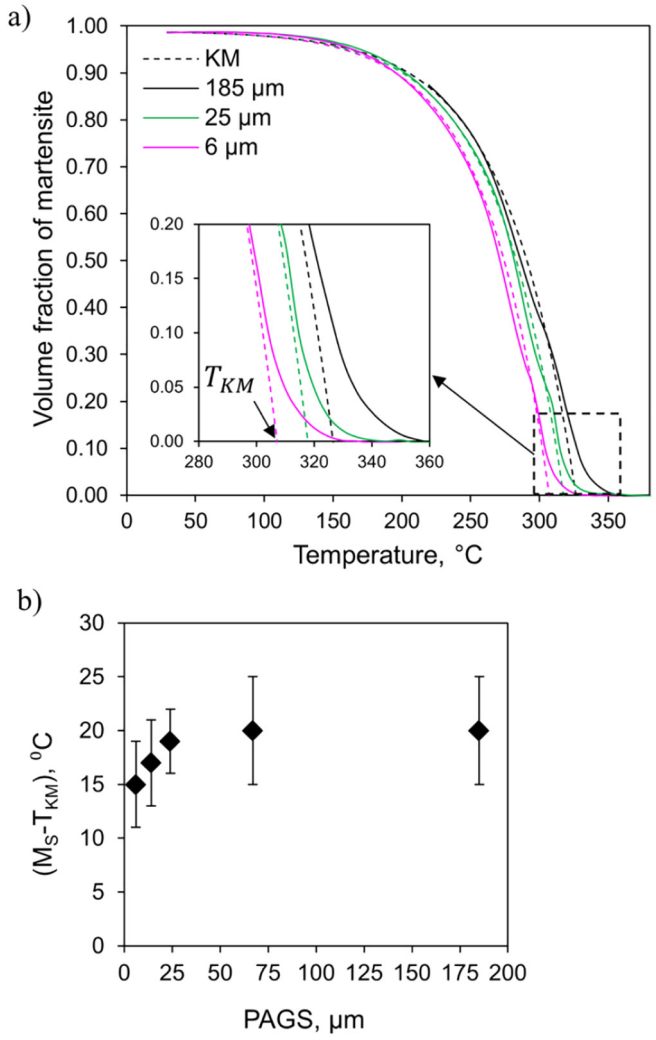

Fig. 5. (a) Experimental volume fraction of martensite (solid lines) and Koistinen-Marburger (KM) fits (dashed lines) against temperature. (b) The shift between M_S and T_{KM} is quantified as a function of the PAGS.

autocatalytically generated nucleation sites. Cohen observed in a low-carbon-Fe-Ni alloy [12] that the autocatalytic factor becomes more important with decreasing PAGS since the forming martensite laths are smaller and more laths have to nucleate in small PAGSs than in large PAGSs to yield the same volume fraction of martensite [40]. The combined effect of both an increased density of grain boundary nuclei and a more pronounced autocatalytic factor causes a faster transformation kinetics (higher transformation rate) at initial stages for small grain sizes compared to larger grain sizes. For this reason, at a given time, microstructures with smaller PAGS form larger fractions of martensite leading to earlier detection by dilatometry.

2. Once the transformation has initiated, austenite grains undergo the so-called *geometrical partitioning process*, explained for the first time by Fisher, Hollomon and Turnbull [6]. The first martensite laths to be formed can freely grow in the undeformed austenite grain. Their length is limited by the PAGS as they cannot cross grain boundaries due to their specific orientation relation with the austenite. The subsequent martensite growth is highly dependent on the distribution of the *elastic strain energy* around the martensite laths and the *stored energy* due to plastic deformation in the austenite caused by the lattice transformation and the shape change.
   - *Elastic strain energy*. As recently shown by two-dimensional phase field modelling of martensitic transformation in stainless steel [41], in PAGSs of 1 μm the highest elastic strains develop parallel to the martensite laths, whereas in larger PAGSs it is along the transverse direction. In small PAGSs, this promotes the repeated nucleation of laths parallel to each other along a single direction favouring the growth of the first variant. Instead, in larger PAGSs, the process happens along multiple directions and at different locations leading to multivariant formation of martensite. According to Kurdjumov-Sachs (K–S) orientations [33], a total of four crystallographically different packets and 24 variants can form within the same austenite grain. Experimentally, multivariant formation of martensite is generally observed to be reduced for PAGS below 10 μm [34,40,42,43].
   - *Stored energy*. The formation of the first block/packet of martensite divides the austenite grain into smaller volumes or γ–pockets. Consequently, subsequent martensite formation takes place in smaller austenite volumes and leads to the formation of smaller blocks/packets that efficiently fill the γ–pockets [28]. This process results in the strengthening of the untransformed austenite through the continuous grain refinement and transformation-induced plastic deformation. The process is known as mechanical stabilisation of the austenite [42–44]. In small-grained microstructures, the untransformed austenite is stronger than that of coarse-grained microstructures. This affects the mechanisms responsible for the decrease of the elastic strain energy arising from the transformation in two manners: the multivariant formation of martensite is reduced or even suppressed and the accommodation of plastic deformation in austenite is more difficult. These two relaxation

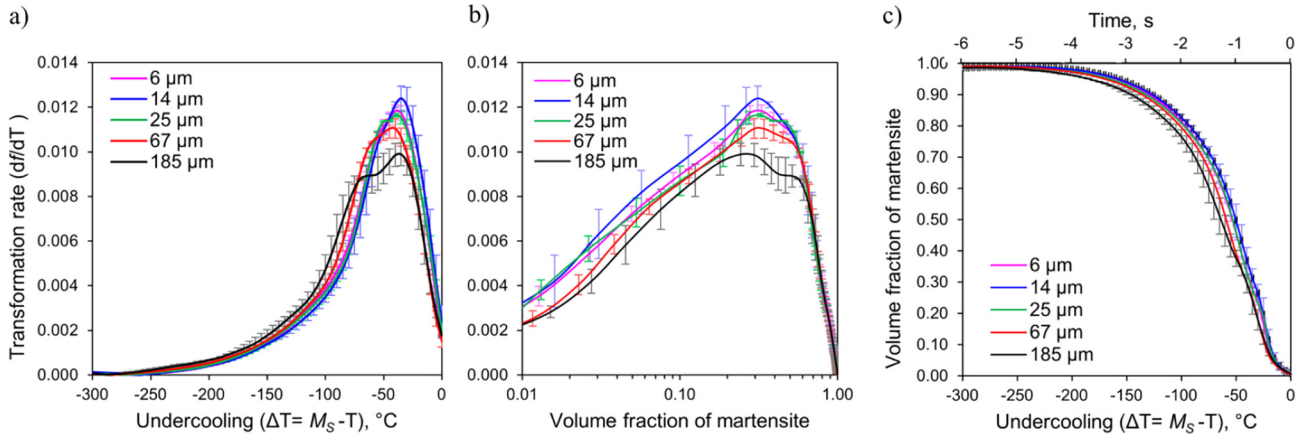

Fig. 6. (a) Martensite transformation rate ($df_{\alpha'}/dT$) against undercooling (ΔT). The transformation starts at zero undercooling, which corresponds to the M_S at which the fraction of formed martensite is $f_{\alpha'} = 0.01$. (b) Transformation rate ($df_{\alpha'}/dT$) against volume fraction of martensite. (c) Volume fraction of martensite against both undercooling and time.

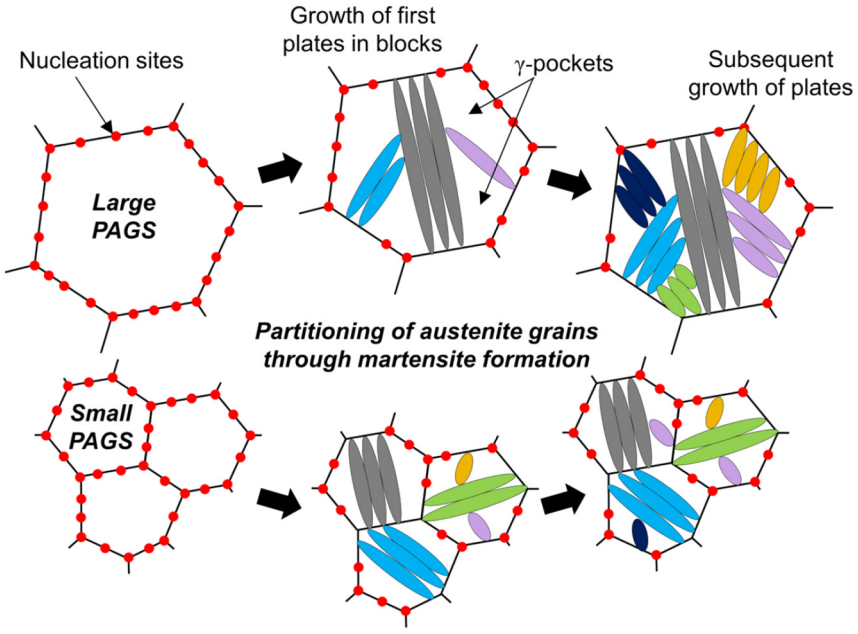

Fig. 7. Schematic drawing comparing the progressive partitioning process of austenite grains by martensite plates in large and small grain sizes. Red dots indicate nucleation sites.

mechanisms are less likely to occur in microstructures with small austenite grain sizes than in large grain sizes and the elastic strain energy is mainly relaxed through the repeated nucleation of martensite laths at the α′/γ interface, as supported by phase field simulations [41]. Therefore, this process has two consequences: 1) the progress of the transformation complies with the increasing undercooling and 2) the elastic strain energy at the α′/γ interface decreases. This results in higher martensite formation rates for small-grained microstructures at initial stages. After the formation of around a 0.30 martensite fraction, the plastic strain accumulated in the surrounding γ–pockets appears to exert a higher resistance against the progress of the transformation and the rate slows down [40,41,43]. Hence, it can be concluded that the strengthening of the austenite phase acts as a main controlling mechanism of the martensite transformation kinetics [16,18]. For this reason, although the nucleation rate is higher in the case of a small PAGS, the transformation rate decreases rapidly as soon as some austenite volume is consumed and larger undercooling is required to overcome the excess strain energy and proceed with the transformation.

4.2. Thermodynamic balance required to form martensite

The diffusionless growth of athermal martensite can in principle occur when the temperature is reduced below T_0, the temperature at which the Gibbs free energies of the parent fcc and the product bcc phase are equal ($G^{\gamma} = G^{\alpha}$). The degree of undercooling required to initiate the transformation ($\Delta T = T_0 - M_S$) depends on the energy balance between the negative contribution of the chemical free energy change due to the formation of a certain volume of martensite ($\Delta G_{chem}^{\gamma\to\alpha} = G^{\alpha} - G^{\gamma}$) and the positive contribution of non-chemical terms opposing the transformation. These non-chemical terms comprise: 1) elastic strain energy (E^{str}), which arises from the shape and volume change that accompanies the phase transformation and is proportional to the volume of the martensite plate; 2) the interfacial energy (σ) that results from the creation of a certain area of α′/γ phase boundary and 3) the energy that is being stored (E^{stored}) in the parent or product phases (as point defects and dislocations) due to plastic deformation caused by the lattice transformation [15,20]. The latter component becomes larger when the austenite becomes stronger because of gradual work hardening during the transformation.

Increasing undercooling below the M_S temperature during cooling implies a favourable energy balance at each temperature to supply sufficient driving force for the transformation $\Delta G_{chem}^{\gamma\to\alpha}$ to overcome the work exerted by an increasingly stronger austenite. In this way, the transformation progresses. As pointed out by Ansell and co-workers [24,25], this work can be directly related to the strength of the austenite phase. The driving force at the M_S temperature is known as critical driving force ($\Delta G_c^{\gamma\to\alpha}$). In relation to the factors mentioned above (E^{str}, σ, E^{stored}), the composition of the alloy and, as evidenced here, the PAGS play a crucial role on the $\Delta G_c^{\gamma\to\alpha}$ value. The balance between critical driving force and the resistance exerted by the austenite against interface motion (W_γ) is expressed by:

$$\Delta G_c^{\gamma\to\alpha}(x_i, M_S) = W_\gamma\left(x_i, E^{str}, \sigma, E^{stored}, d^{\gamma}\right) \tag{2}$$

in which x_i denotes the composition of the alloy and d^{γ} stands for the PAGS. The terms in Eq. (2) are evaluated in the following paragraphs.

4.2.1. Critical driving force change and austenite grain refinement

As is shown by the experimental results in Fig. 4, the M_S temperature decreases with decreasing PAGS. Fig. 8 shows the Gibbs free energy change ($\Delta G^{\gamma\to\alpha}$) as a function of temperature calculated using ThermoCalc software (TCFE9 database) for the steel under investigation. The change in critical driving force related to grain size (ΔG_c^{gr}) was evaluated using the experimental M_S temperatures for the smallest and largest PAGSs. A critical driving force of about 1570 J/mol is required for the transformation of a microstructure with a PAGS of 185 μm, while 1800 J/mol is needed for the microstructure with a PAGS of 6 μm. This means that an extra driving force of 230 J/mol is needed due to the grain refinement from 185 to 6 μm.

An approximately constant change in driving force with the temperature is observed at temperatures near the M_S temperatures. A good linear fit with a slope of $(\Delta G/\Delta T)_{M_S} = 7.36$ J mol^{-1} K^{-1} is found in the shaded region in Fig. 8 ($R^2 = 0.9998$). This fact allows the driving force to be expressed as a linear function of the M_S temperature:

$$\Delta G_c^{\gamma\to\alpha} = \left({}^{\Delta G}/_{\Delta T}\right)_{M_S} \cdot (T_1 - M_S) \tag{3}$$

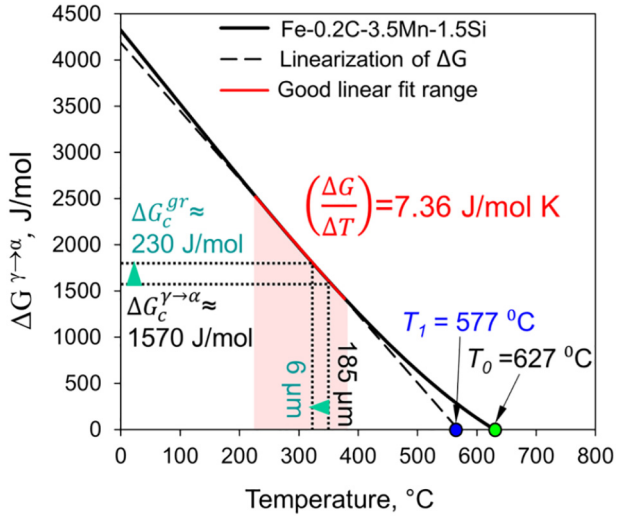

Fig. 8. Driving force as a function of temperature calculated with ThermoCalc (TCFE9 database). The critical driving force for PAGSs of 185 μm is noted. ΔG^{gr} stands for the increment in the driving force due to grain refinement from 185 to 6 μm.

where T_1 is the intercept with the x-axis. A similar linear relationship was observed by Van Bohemen et al. [27] for Fe-C alloys with carbon contents of 0.1–0.7 wt. %, for which an average value of $(\Delta G/\Delta T)_{M_s} = 7.22\ \mathrm{J\ mol^{-1}\ K^{-1}}$ was found.

4.2.2. Austenite work opposing the martensite growth

Martensite growth is controlled by the mobility of the semi-coherent interface that exists between the martensite and the austenite matrix. As the term on the right side of Eq. (2) describes, the austenite resistance against interface motion depends on the strain energy, the interfacial energy, the composition of the alloy and the PAGS. This can be formally formulated as:

$$W_\gamma = K_1\left(E^{str}, \sigma\right) + W_\mu(x_i) + W_{HP}\left(d^\gamma\right) + W_C\left(d^\gamma, E^{stored}\right) \quad (4)$$

where K_1 is a constant that depends on the strain and interfacial energies, W_μ is the athermal frictional work, W_{HP} is the work due to Hall-Petch grain-size effect and W_C is the stored energy. The first two terms were proposed by Ghosh and Olson [13,14] to formulate the austenite resistance against the interface motion in thermodynamic terms. Recently, additional two terms (W_{HP}, W_C) have been introduced by Van Bohemen and co-authors [27] in an extension of Ghosh and Olson's thermodynamic model to account for grain size. The meaning of each term is explained as follows:

a) The athermal frictional work (W_μ) represents the lattice friction experienced by the interfacial dislocations due to interface motion during martensite growth. It was initially described based on solid solution strengthening by Ghosh and Olson [14]. For multicomponent steels it follows a quadratic type superposition law:

$$W_\mu = K_\mu^C \cdot x_C^{0.5} + \sqrt{\sum_i {K_\mu^i}^2 \cdot x_i} \quad (5)$$

in which the summation runs over the other alloying elements, besides carbon, and x_i stands for the content of alloying element i in wt. %. The coefficients (K_μ^i) are shown in Table 2.

b) One of the main austenite strengthening mechanisms is the Hall-Petch effect (W_{HP}), by which grain refinement would lead to the mechanical stabilisation of the austenite. As proposed by Ansell and co-workers [24,25], the mechanical stabilisation is due to the increase of the locally stronger grain volume next to the grain boundary relative to the decrease of the locally softer inner grain volume. The work is reciprocally proportional to the square root of the austenite grain size (d^γ), as displayed by:

$$W_{HP} = K_{HP}/\sqrt{d^\gamma} \quad (6)$$

The proportionality constant is $K_{HP} = 350\ \mathrm{J\,\mu m^{1/2}/mol}$, as derived and validated using data of approximately 100 alloys in reference [27].

c) W_C concerns the increase in the stored energy due to the formation of martensite laths with large c/a (width/length) aspect ratio. As previously found by transmission electron microscopy in low carbon steels, the lath width remains essentially constant and independent of the PAGS, whereas the length of martensite laths scales with the PAGS [32,33,40]. The semi-coherent interface that forms between austenite and martensite is flat when the martensitic transformation is unconstrained; however, when the transformation is constrained by its surroundings as it occurs with austenite grain refinement, the need to minimise strains introduces some curvature in the interface [19]. This leads to more equiaxed laths, *i.e.* higher c/a aspect ratios, where the curvature of the semi-coherent α'/γ interface is more pronounced. This results in a higher stored energy in the surrounding austenite due to the increase of dislocations density at the phase boundary needed to accommodate the curvature. This effect appears to be strong for low PAGSs [11,20]. This stored energy is expressed by:

$$W_C = K_C\ \exp\left(-6 \cdot d^\gamma / d_w^\gamma\right) \quad (7)$$

where the proportionality constant is $K_C = 370$ J/mol [27] and d_w^γ is a rate parameter in terms of the grain-size dependence of W_C.

Table 2
The coefficients K_μ of the interfacial frictional work (W_μ) for the martensite/austenite semi-coherent interface [27].

Element	C	Mn	Si	Cr	Mo
K_μ^i(J/mol)	670	195	140	170	205

4.3. Thermodynamic M_S-model considering the PAGS

The thermodynamic expression that accounts for the influence of the PAGS on the critical driving force for the martensitic transformation is found by equating Eqs. (3) and (4):

$$\left({}^{\Delta G}/_{\Delta T}\right)_{M_S} \cdot (T_1 - M_S) = K_1 + W_\mu\left(K_\mu^i\right) + W_{HP}\left(K_{HP}, d^\gamma\right) + W_C\left(K_C, d^\gamma, d_w^\gamma\right) \quad (8)$$

The values of the parameters K_1 and d_w^γ are not known. Here, a methodology is developed for their selection and interpretation in order to propose a fully-physically based M_S-model that considers the influence of the PAGS.

4.3.1. The prior austenite grain size rate parameter (d_w^γ)

The distributions of c/a, the lath aspect ratio, shown in Fig. 3 for different PAGSs reveal that austenite microstructures with low PAGS give rise to a tendency for equiaxed martensite laths or, in other words, to high c/a lath aspect ratios. A direct consequence of the increase of the c/a aspect ratio is a more pronounced curvature of the martensite/austenite interface, which leads to a raise of the elastic strain energy due to higher density of interface dislocations and coherency strain. Calculations by Christian [11] based on linear elastic theory provide values of

$E^{str} = 2000–5000$ J/mol for $c/a \leq 0.05$, which values are higher than the actual driving force for the martensitic transformation (1500–1800 J/mol) [43]. This suggests that relaxation mechanisms, such as plastic deformation and self-accommodating blocks/packets through multivariant formation play an important role in lowering the stored energy, which enables the progress of the transformation. Although crystallographic aspects of the martensite substructure have been extensively investigated in the literature, morphological features such as block lengths and widths are not very often analysed in a quantitative manner for grain sizes below 20 μm [33,40,45]. Hidalgo and Santofimia [34] characterized using EBSD martensitic microstructures with PAGS of 80, 14, 10.3 and 9.2 μm in a low-carbon steel of similar composition to the present case and quantified a decrease in the PAGS/packet size ratio in more than a 50% for PAGS of 14 μm or smaller with respect to a PAGS of 80 μm. These observations show consistency with the results of the present study (Fig. 3) and support the selection of a $d_w^{\gamma} = 14$ μm.

4.3.2. Elastic strain, interfacial energy and defect size in the K_1 constant

The K_1 term in Eq. (8) is described in the literature as a constant with a value of about 1050 J/mol. It depends on the elastic strain energy (E^{str}), the interfacial energy (σ) and the defect size, as defined by Olson and Cohen's dislocation model for the description of heterogeneous nucleation of bcc-martensite on pre-existing defects or stacking faults in fcc-austenite [9,10]. It can be formulated as:

$$K_1 = E^{str} + \frac{2\sigma}{n\rho_A} \tag{9}$$

where $n\rho_A$ defines the defect size as the product between the number n of planes constituting the thickness of the fault and the atomic density per unit area of fault plane (ρ_A). In the case of an fcc-to-bcc transformation, the fault resembles a bcc structure and it is the result of the dissociation of fcc Shockley partial dislocations, described by Olson and Cohen [9]. Provided that the driving force is sufficient, the stacking fault energy (γ) becomes negative and faults form favourably on closest-packed planes at crystal defects (such as grain and phase boundaries) by dissociation of groups of existing dislocations. The stacking fault energy depends on the chemical free energy change between martensite and austenite ($\Delta G_{chem}^{\gamma\rightarrow\alpha}$) the elastic strain energy and the true interfacial energy (σ) that determine the fault size by: $\gamma = n\rho_A(\Delta G_{chem}^{\gamma\rightarrow\alpha} + E^{str}) + 2\sigma(n)$. Therefore, the critical condition in which martensite would nucleate at these faults through a barrier-less process ($\gamma = 0$) allows the critical defect size (n^*) to be estimated as:

$$n^* = \frac{2\sigma}{-\rho_A(\Delta G_{chem}^{\gamma\rightarrow\alpha} + E^{str})} \tag{10}$$

Adopting a value of $\Delta G_{chem}^{\gamma\rightarrow\alpha} = -1800$ J/mol, which corresponds to the largest PAGS for the steel under investigation at $T = M_S$, and typical values of elastic strain energy ($E^{str} = 450$ J/mol) and semi-coherent interfacial energy ($\sigma = 0.15$ J/m^2), a critical defect size of $n^* \approx 20$ is obtained. This value is similar to those reported by Olson and Cohen for various binary and ternary Fe-based alloys [9,10]. Substitution of these values in Eq. (9) yields $K_1 \approx 900$ J/mol, which is 110 J/mol lower than the value reported by Olson and Cohen.

Fig. 9 shows that the prediction using the M_S-model, represented by Eq. (8), accurately matches the experimental change in M_S temperature detected with the variation of PAGS for the steel under investigation. All parameters can be physically interpreted and calculated as proposed in this work. Fig. 9 shows that the model captures the more pronounced change in M_S for PAGS below 25 μm. PAGS of 25 μm and lower are usually obtained by annealing near the A_{C3} temperature, as typically done in thermal treatments for the design of ultra-high strength steels. Therefore, this model can be used to optimise the microstructural design of these kinds of steels that involve the controlled formation of martensite

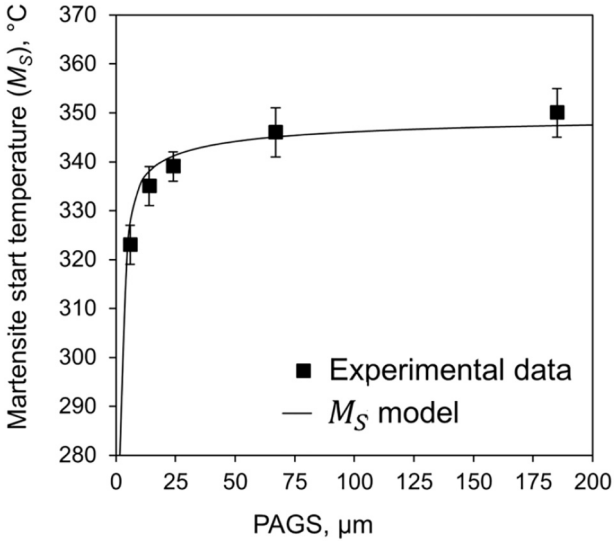

Fig. 9. Evolution of the experimental M_S temperatures with the PAGS and comparison with the M_S model.

phase, such as Quenching and Partitioning steels [4] and other multiphase advanced high strength steels [5], since it allows for a finer adjustment of the thermal treatment. Some considerations to account for when applying the model are the selection of the PAGS rate parameter (d_w^{γ}) and the calculation of the K_1 term. In principle, the PAGS rate parameter suggested in this work should be valid for low-carbon steels with similar content of substitutional elements. However, morphological changes in the martensite substructure are expected with substantial increase of carbon, nickel or chromium [46,47] which can affect the d_w^{γ} value. On the other hand, it has been observed that the position of the modelled curve is very sensitive to the K_1 value, so K_1 can be accurately determined by fitting. A value $K_1 = 1010$ J/mol (instead of 900 J/mol), as proposed in the literature [13], shifts the predictions to lower temperatures by approximately 25 °C, resulting in a poor agreement between the experimental data and the M_S-model. There seems to be a strong link between the critical driving force, the defect size and the K_1 parameter and, thus, it has to be critically considered as it might change depending on the thermodynamic databased used for the Gibbs free energy calculations.

5. Conclusions

This study investigates the influence of the prior austenite grain size (PAGS) on the martensitic transformation in a low-carbon steel. Grain refinement shifts the martensite start temperature (M_S) to lower values. However, it also accelerates the transformation rate at initial stages due to the higher density of nucleation sites provided by a larger grain boundary area. Thus, the formation of similar fractions of martensite requires smaller undercooling (lower times) in fine-grained than in coarse-grained microstructures. This is reflected in a small increase of the Koistinen-Marburger (KM) rate parameter (α_m) and lower deviations between M_S and the KM start temperature as the PAGS decreases. On the other hand, after the formation of a certain fraction of martensite, the transformation rate decreases rapidly in small-grained microstructures due to a significant strengthening of the austenite through: 1) the Hall-Petch grain-size effect; 2) the formation of more equiaxed martensite laths for low PAGS; 3) the suppression of self-accommodation by multivariant formation and thus of strain energy relaxation. These factors contribute to an increase of austenite work against the movement of the martensite/austenite interface (progress of the transformation), which in combination with the solid solution frictional work exerted by the austenite lattice and the elastic strain and interfacial energies explain the experimental decrease in M_S

observed when the PAGS is reduced from 185 to 6 μm. Experimental observations are thermodynamically explained through the M_S-model, where all required parameters can be obtained and interpreted on a physical basis and which allows for the prediction of PAGS effect on the martensite formation kinetics. These results enable the optimisation of microstructural design of advanced high strength steels that involve the formation of a controlled fraction of martensite.

CRediT authorship contribution statement

Carola Celada-Casero: Conceptualization, Methodology, Validation, Formal analysis, Investigation, Writing - original draft, Visualization. **Jilt Sietsma:** Writing - review & editing, Supervision, Project administration, Funding acquisition. **Maria Jesus Santofimia:** Conceptualization, Resources, Writing - review & editing, Supervision, Project administration, Funding acquisition.

Acknowledgments

The authors deeply acknowledge the support from the Research Fund for Coal and Steel for funding this research under the Contract RFCS-02-2015 (Project No. 709755). C. Celada-Casero thanks Kees Kwakernaak for his support with the EBSD measurements.

Data availability

The raw and processed data required to reproduce these findings are available to download from https://doi.org/10.4121/uuid:bb8859ef-e101-4043-afe7-a910bd1184a6.

References

[1] J.W. Morris Jr., Making steel strong and cheap, Nat. Mater. 16 (2017) 787–789.
[2] M. Koyama, Z. Zhang, M. Wang, D. Ponge, D. Raabe, K. Tsuzaki, et al., Bone-like crack resistance in hierarchical metastable nanolaminate steels, Science 355 (2017) 1055–1057.
[3] F.G. Caballero, H.K.D.H. Bhadeshia, Very strong bainite, Curr. Opin. Solid State Mater. Sci. 8 (2004) 251–257.
[4] M.J. Santofimia, L. Zhao, R. Petrov, C. Kwakernaak, W.G. Sloof, J. Sietsma, Microstructural development during the quenching and partitioning process in a newly designed low-carbon steel, Acta Mater. 59 (2011) 6059–6068.
[5] A. Navarro-López, J. Sietsma, M.J. Santofimia, Effect of prior athermal martensite on the isothermal transformation kinetics below Ms in a low-C high-Si steel, Metall. Mater. Trans. A 47 (2016) 1028–1039.
[6] J.C. Fisher, J.H. Hollomon, D. Turnbull, Kinetics of the austenite to martensite transformation, Trans. AIME 185 (1949) 691–700.
[7] D.P. Koistinen, R.E. Marburger, A general equation prescribing the extent of the austenite-martensite transformation in pure iron-carbon alloys and plain carbon steels, Acta Metall. 7 (1959) 59–60.
[8] A.R. Entwisle, The kinetics of martensite formation in steel, Metall. Trans. 2 (1971) 2395–2407.
[9] G.B. Olson, M. Cohen, A general mechanism of martensitic nucleation: part II. FCC → BCC and other martensitic transformations, Metall. Trans. A. 7 (1976) 1905–1914.
[10] G.B. Olson, M. Cohen, A general mechanism of martensitic nucleation: part I. General concepts and the FCC → HCP transformation, Metall. Trans. A. 7 (1976) 1897–1904.
[11] J.W. Christian, in: G.B. Olson, M. Cohen (Eds.), Thermodynamics and Kinetics of Martensite, ICOMAT. MIT, Boston, MA 1979, pp. 145–154.
[12] M. Cohen, Martensitic nucleation - revisited, Mater. Trans. JIM 33 (1992) 178–183.
[13] G. Ghosh, G.B. Olson, Kinetics of F.C.C. → B.C.C. heterogeneous martensitic nucleation —I. The critical driving force for athermal nucleation, Acta Metall. Mater. 42 (1994) 3361–3370.
[14] G. Ghosh, G.B. Olson, Kinetics of F.C.C. → B.C.C. heterogeneous martensitic nucleation —II. Thermal activation, Acta Metall. Mater. 42 (1994) 3371–3379.
[15] J.W. Christian, Kinetics of Martensitic Transformations. The Theory of Transformations in Metals and Alloys, Pergamon, Oxford, 2002 1062–1075.
[16] S.M.C. Van Bohemen, J. Sietsma, Martensite formation in partially and fully austenitic plain carbon steels, Metall. Mater. Trans. A 40 (2009) 1059–1068.
[17] S.M.C. van Bohemen, J. Sietsma, Effect of composition on kinetics of athermal martensite formation in plain carbon steels, Mater. Sci. Technol. 25 (2009) 1009–1012.
[18] S.M.C. van Bohemen, J. Sietsma, Kinetics of martensite formation in plain carbon steels: critical assessment of possible influence of austenite grain boundaries and autocatalysis, Mater. Sci. Technol. 30 (2014) 1024–1033.
[19] H. Bhadeshia, R. Honeycombe, Chapter 5 - formation of martensite, in: H. Bhadeshia, R. Honeycombe (Eds.), Steels: Microstructure and Properties, Fourth editionButterworth-Heinemann 2017, pp. 135–177.
[20] H.K.D.H. Bhadeshia, Developments in martensitic and bainitic steels: role of the shape deformation, Mater. Sci. Eng. A 378 (2004) 34–39.
[21] S. Karewar, J. Sietsma, M.J. Santofimia, Effect of pre-existing defects in the parent fcc phase on atomistic mechanisms during the martensitic transformation in pure Fe: a molecular dynamics study, Acta Mater. 142 (2018) 71–81.
[22] H.-S. Yang, H.K.D.H. Bhadeshia, Austenite grain size and the martensite-start temperature, Scr. Mater. 60 (2009) 493–495.
[23] T. Hanamura, S. Torizuka, S. Tamura, S. Enokida, H. Takechi, Effect of austenite grain size on transformation behavior, microstructure and mechanical properties of 0.1C–5Mn martensitic steel, ISIJ Int. 53 (2013) 2218–2225.
[24] T.J. Nichol, G. Judd, G.S. Ansell, The relationship between austenite strength and the transformation to martensite in Fe-10 pct Ni-0.6 pct C alloys, Metall. Trans. A. 8 (1977) 1877–1883.
[25] P.J. Brofman, G.S. Ansell, On the effect of fine grain size on the Ms temperature in Fe-27Ni-0.025C alloys, Metall. Trans. A. 14 (1983) 1929–1931.
[26] S.-J. Lee, K.-S. Park, Prediction of martensite start temperature in alloy steels with different grain sizes, Metall. Mater. Trans. A 44 (2013) 3423–3427.
[27] S.M.C. van Bohemen, L. Morsdorf, Predicting the Ms temperature of steels with a thermodynamic based model including the effect of the prior austenite grain size, Acta Mater. 125 (2017) 401–415.
[28] J.R.C. Guimarães, P.R. Rios, Unified model for plate and lath martensite with athermal kinetics, Metall. Mater. Trans. A 41 (2010) 1928–1935.
[29] R.A. Grange, The rapid heat treatment of steel, Metall. Trans. 2 (1971) 65–78.
[30] B.D. Cullity, C.D. Graham, Introduction to Magnetic Materials, 2nd ed. IEEE/Wiley, Hoboken, N.J., 2009
[31] D. San Martín, Y. Palizdar, R.C. Cochrane, R. Brydson, A.J. Scott, Application of Nomarski differential interference contrast microscopy to highlight the prior austenite grain boundaries revealed by thermal etching, Mater. Charact. 61 (2010) 584–588.
[32] S. Morito, H. Yoshida, T. Maki, X. Huang, Effect of block size on the strength of lath martensite in low carbon steels, Mater. Sci. Eng. A 438–440 (2006) 237–240.
[33] S. Morito, H. Tanaka, R. Konishi, T. Furuhara, T. Maki, The morphology and crystallography of lath martensite in Fe-C alloys, Acta Mater. 51 (2003) 1789–1799.
[34] J. Hidalgo, M.J. Santofimia, Effect of prior austenite grain size refinement by thermal cycling on the microstructural features of as-quenched lath martensite, Metall. Mater. Trans. A (2016) 1–14.
[35] S.M.C. van Bohemen, The nonlinear lattice expansion of iron alloys in the range 100–1600 K, Scr. Mater. 69 (2013) 315–318.
[36] T. Sourmail, V. Smanio, Determination of Ms temperature: methods, meaning and influence of 'slow start' phenomenon, Mater. Sci. Technol. 29 (2013) 883–888.
[37] S. Ramesh Babu, D. Ivanov, D. Porter, Influence of microsegregation on the onset of the martensitic transformation, ISIJ Int. 59 (2018) 169–175.
[38] O. Krisement, E. Houdremont, F. Wever, Contribution a la thermodynamique de la transformation austenite-martensite dans les alliages fer-carbone, Rev. Metall. 51 (1954) 401–410.
[39] G.B. Olson, M. Cohen, Kinetics of strain-induced martensitic nucleation, Metall. Trans. A. 6 (1975) 791.
[40] S. Morito, H. Saito, T. Ogawa, T. Furuhara, T. Maki, Effect of austenite grain size on the morphology and crystallography of lath martensite in low carbon steels, ISIJ Int. 45 (2005) 91–94.
[41] H.K. Yeddu, Phase-field modeling of austenite grain size effect on martensitic transformation in stainless steels, Comput. Mater. Sci. 154 (2018) 75–83.
[42] T. Furuhara, K. Kikumoto, H. Saito, T. Sekine, T. Ogawa, S. Morito, et al., Phase transformation from fine-grained austenite, ISIJ Int. 48 (2008) 1038–1045.
[43] S. Takaki, K. Fukunaga, J. Syarif, T. Tsuchiyama, Effect of grain refinement on thermal stability of metastable austenitic steel, Mater. Trans. 45 (2004) 2245–2251.
[44] S. Chatterjee, H.S. Wang, J.R. Yang, H.K.D.H. Bhadeshia, Mechanical stabilisation of austenite, Mater. Sci. Technol. 22 (2006) 641–644.
[45] S. Morito, Y. Edamatsu, K. Ichinotani, T. Ohba, T. Hayashi, Y. Adachi, et al., Quantitative analysis of three-dimensional morphology of martensite packets and blocks in iron-carbon-manganese steels, J. Alloys Compd. 577 (2013) S587–S592.
[46] M. Umemoto, E. Yoshitake, I. Tamura, The morphology of martensite in Fe-C, Fe-Ni-C and Fe-Cr-C alloys, J. Mater. Sci. 18 (1983) 2893–2904.
[47] G. Krauss, A.R. Marder, The morphology of martensite in iron alloys, Metall. Trans. 2 (1971) 2343–2357.